Hindawi
Journal of Nanomaterials
Volume 2023, Article ID 5485632, 11 pages
https://doi.org/10.1155/2023/5485632

Research Article

Radiosensitivity Enhancement using Triptorelin Conjugated Bismuth Sulfide Nanoparticles (Bi_2S_3@BSA) in Radiotherapy for Breast Cancer Cells

Yazdan Choghazardi,[1] **Hosein Azimian**,[1] **Alireza Montazer Abadi**,[1] **Milad Mohammadi Khoshisani**,[1] **Fereshteh Vaziri Nezamdoust**,[1,2] **and Hamid Gholamhosseinian**[1]

[1]*Department of Medical Physics, Faculty of Medicine, Mashhad University of Medical Sciences, Mashhad, Iran*
[2]*Department of Applied Cell Science, Faculty of Advanced Medical Sciences, Tabriz University of Medical Sciences, Tabriz, Iran*

Correspondence should be addressed to Hamid Gholamhosseinian; gholamhosseinianh@mums.ac.ir

Received 9 November 2022; Revised 6 February 2023; Accepted 8 April 2023; Published 6 May 2023

Academic Editor: Jagpreet Singh

The aim of this study was to assess the radiosensitivity of bismuth sulfide nanoparticles conjugated with a synthetic agonist analog of gonadotropin-releasing hormones in targeted radiotherapy for breast cancer. After synthesis and characterization of nanoparticles, cytotoxicity of nanoparticles was measured by MTT assay, and the survival fraction was determined by colony formation assay. Finally, flow cytometry was performed to identify the mechanism of radiosensitization. Characterization results determined the spherical shape of Bi_2S_3@BSA with an average size of 8.649 ± 1.6 nm, and Fourier transform infrared confirmed the successful binding of triptorelin to the surface of the nanoparticles. MTT test results show that the Bi_2S_3@BSA–triptorelin did not cause any toxicity ($P < 0.05$) even up to 75 μg/ml. At all doses of ionizing radiation, colony formation assays showed that the nontoxic concentration of Bi_2S_3@BSA–triptorelin significantly increased cell death in MCF-7 cells compared to Bi_2S_3@BSA ($P < 0.05$). The apoptosis test also confirmed colony formation assay results at all doses and introduced apoptosis as a mechanism of radiosensitivity produced by nanoparticles. Certainly, targeted bismuth sulfide nanoparticles can be a good candidate for increasing radiosensitivity against tumor cells.

1. Introduction

Cancer is one of the leading causes of death in humans. Therefore, cancer treatment is currently a major challenge [1]. Common cancer treatments include surgery, radiation therapy (RT), chemotherapy, hormonal therapy, or combination therapy [2]. RT is commonly used to treat over 50% of cancer patients [3] and 80%–90% of breast cancer patients [4]. Although RT has significant advantages, it is a nonselective technic because radiation cannot distinguish between normal and cancer cells; therefore, the beam must be confined to the target volume [5]. To overcome this disadvantage, different strategies, such as tomotherapy, image-guided radiotherapy, and intensity-modulated radiotherapy, can be used to deliver the maximum dose to tumor tissue while protecting surrounding normal tissue [4, 6]. However, the equipment-based solution to increase the quality of RT may be limited because a more accurate irradiation volume can lead to excluding significant undetectable cancer cells [7]. Improves tumor response to radiation is another mechanism for enhancement of the radiotherapy ratio [8]. It is possible with a different mechanism, such as using radiosensitizer compounds [9] and molecular regulators of mRNAs (miRNA) [10]. As a definition, when used in combination with radiation, radiosensitizer compounds enhance the death of cancer cells while having a minimal effect on healthy tissue [11]. In recent years, advances in tumor therapy have been attained through methods such as enhanced cellular internalization (using nanoparticles less than 500 nm in diameter) [12]. Strategies based on nanomaterial-mediated tumor radiosensitization are mainly adopted to improve the energy deposition of ionizing radiation in the irradiated volume. This can accelerate the production of

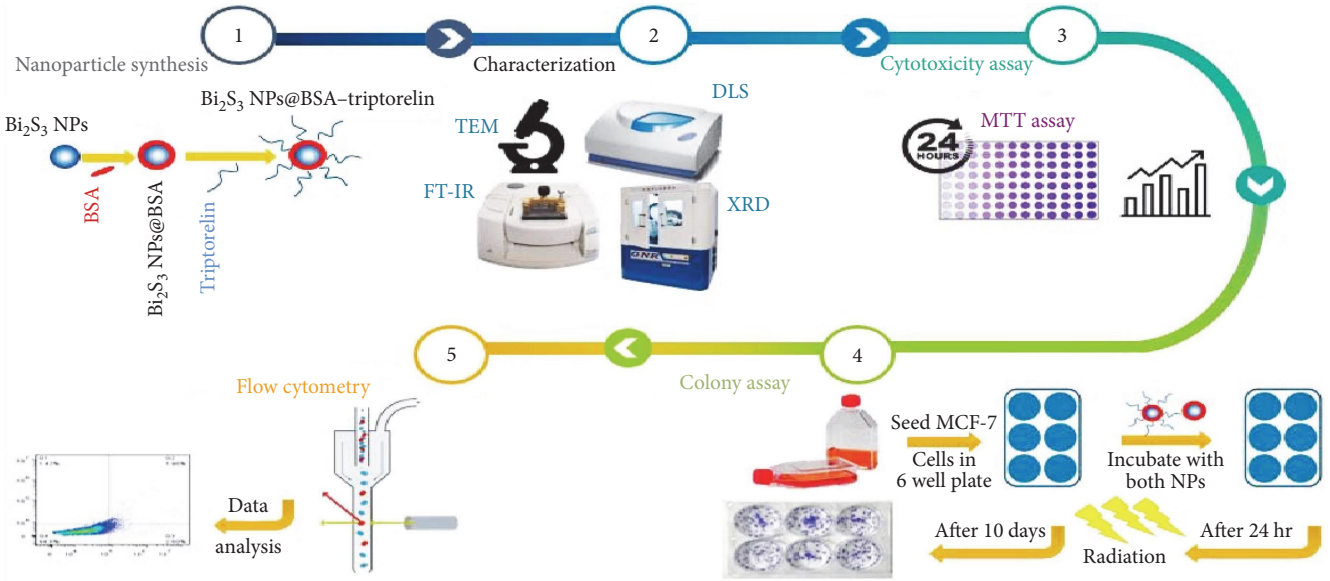

FIGURE 1: Schematic illustration of targeted Bi_2S_3@BSA NPs as a targeted radiosensitizer for radiotherapy.

reactive oxygen species to make cancer cells more sensitive to radiation [13]. Since metal nanoparticles, such as gold, platinum, and bismuth, showed radio-enhancing specifications [14]. Nanoparticles' internalization into tumor tissue could elevate localized energy deposition through free electrons and radical species. As a result, a similar degree of tumor destruction is achieved with lower radiation doses [15]. Among the high atomic number nanoparticles, bismuth (the heaviest stable nonradioactive element) is a better candidate as a radiosensitizer which improves the quality of RT compared to other nanoparticles [14] since, as one of the heaviest metal atoms, it has shown low toxicity, has a high electron density and is appropriate to absorb ionizing X-ray [16]. Another important advantage is that it is (until 2016) ~2,000 times less expensive than gold per mole [17]. In comparison to other nanoparticles (like gold), bismuth nanoparticles can better act as radiosensitizers to elevate the radiation dose delivered to tumors. This is because the number of photoelectric interactions is more [18]. Conventional drug-based radiosensitizers that do not have an efficient targeting function are most effective at the tumor site, but radiosensitivity heavily depends on the accurate localization of the radiosensitizers to cancer cells [19]. Paul Ehrlich introduced the concept of targeted drugs. This hypothesis states that tumors have specific antigens and that some factors, such as antibodies, can enhance drug delivery to tumor sites and kill them [20]. Biomolecules that bind to the surface of nanoparticles can interact with their receptors on the cell's plasma membrane. This phenomenon can be used to engineer the surface of nanoparticles with specific functional ligands (such as antibodies, proteins, or peptides) to target-specific receptors on the cell surface for medical purposes [21, 22]. Peptides are inexpensive, have higher activity per mass compared to antibodies, are more stable at room temperature, are more tissue-penetrating (to tumors or organs), and induce immune responses to antibodies [23, 24]. Peptide-conjugated metal nanoparticles have been shown to selectively attack tumor cells without affecting normal tissues [25]. Triptorelin (pGlu-His-Trp-Ser-Tyr-DTrp-Leu-Arg-Pro-Gly-NH_2) is a species of LHRH (luteinizing hormone-releasing hormone) receptor agonist whose action mechanism and affinity for binding to LHRH or GnRH (gonadotropin-releasing hormone) receptors is similar to natural LHRH [26]. Moreover, direct antiproliferative effects of the triptorelin in breast cancer cells that express GnRH receptors (such as MCF-7) have been demonstrated [27]. An ideal radiosensitizer should enhance the efficacy of RT by inducing radiosensitivity, good tumor-targeting ability, and low toxicity [19]. Herein, efforts were made to develop a novel targeted-radiosensitizer by targeting the GnRH receptors on the surface of MCF-7 cells (studies showed that the expression of these receptors and specific binding sites for LHRH analog in the membrane of MCF-7 cells had been determined) [27, 28] in order to enhance the quality and minimize the side effects of RT. In this study, we investigated the cytotoxicity, radiosensitization effects, and mechanism of radiosensitivity of targeted Bi_2S_3@BSA NPs with Triptorelin after treatment with a 6 MV photon beam in MCF-7 cell line (Figure 1).

2. Materials and Methods

2.1. Synthesis of Bi_2S_3@BSA NPs Conjugated with Triptorelin. Aqueous bismuth nitrate of 2.8 ml in 3 M HNO_3 solution at a concentration of 25 mM and a temperature of 25°C was introduced dropwise into 40 ml BSA solutions at a concentration of 66 mg/ml and a temperature of 25°C under vigorous stirring in less than 2 min. After 2 min, 6 ml NaOH solution (5 M) was added at a single instance, and the color of the solution began to change from pale yellow to light brown and then to dark black in 10 min. All synthesis steps were performed at room temperature. After 12 hr aging,

the resulting compound was centrifuged at 12,000 rpm for 15 min. Finally, in order to purify synthesized nanoparticles, they were dialyzed for 48 hr against Milli-*Q* water to eliminate any possible debris. To conjugate Bi_2S_3@BSA with triptorelin, 1 ml of the synthesized nanoparticles was placed on a magnetic stirrer (6.5 pH), then 0.5 mg of triptorelin peptide was added. Finally, 0.15 mg of EDC (carbodiimide hydrochloride) and 0.09 mg of NHS (*N*-hydroxysulfosuccinimide) were added. The resulting mixture was stirred at room temperature for 2 hr. Finally, the resulting compounds were dialyzed for 24 hr in a refrigerator.

2.2. Characterization of NPs. A transmission electron microscope (Philips (CM120)) was used to determine the size and morphology of the Bi_2S_3@BSA NPs. X-ray diffraction is a fundamental and important characterization technique that is used to analysis of all materials. To confirm the Microstructure of NPs (GNR EXPLORER) with Cu-Kα radiation ($k = 1.542$ A) with the Bragg angle ranging from 10° to 80°, X-ray diffraction was used.

The zeta potential of NPs was measured using a nano/zeta sizer (HORIBA SZ100) with 25 scans in each spectrum, and the size of NPs was assessed by dynamic light scattering (HORIBA SZ100) in an aqueous solution. In addition, to measure nanoparticle stability in the cellular environment, Bi_2S_3@BSA–triptorelin NPs were suspended in the RPMI 1640 + 10% FBS and incubated for 24 hr at 37°C. Then the behavior of the Bi_2S_3@BSA–triptorelin NPs was measured by dynamic light scattering. Fourier transform infrared (FT-IR) spectroscopy was performed to determine the chemical structure of samples (Thermo Nicolet (AVATAR 370 FT-IR (USA))).

2.3. Cell Culture. Human breast adenocarcinoma (MCF-7) cell lines, obtained from the Pasteur Institute of Iran, were used in the in vitro study. MCF-7 cell lines were cultured in RPMI 1640 (Roswell Park Memorial Institute) supplemented with 10% fetal bovine serum (FBS) (Gibco, USA) and 1% penicillin-streptomycin (Gibco, USA). Subculturing of the MCF-7 cell lines was performed by detaching the adherent cells using 0.025% trypsin-EDTA (Gibco, USA). In order to wash the flask and remove the debris and floated dead cells, plates, and flasks were washed with phosphate-buffered saline (PBS) (Gibco, USA). Cells were incubated at 37°C with humidified 5% CO_2. In this study, before performing all the experiments, cells were carefully observed under a microscope. Also, all experiments were performed in the cell logarithmic growth stage.

2.4. Cytotoxicity Tests. Cytotoxicity test was performed by MTT (2,5-diphenyl-2H-tetrazolium bromide) assay as follows: an optimal number of MCF-7 cells were seeded in two 96-well plates (density of 104 per well [29]) and incubated in a RPMI 1640 supplemented with 10% FBS and 1% penicillin-streptomycin at 37°C and 5% CO_2 atmosphere 24 hr before treatment to allow attachment. The next step was to remove the culture medium and wash the plates with PBS. Then, the cells were incubated with 200 μl culture medium (5% FBS) per well containing Bi_2S_3@BSA, Bi_2S_3@BSA–triptorelin NPs at a series of concentrations (0 (control) 5, 10, 15, 25, 50, 75, 100, 150, and 200 μg/ml) for 24 hr. After that, the cells were washed twice with PBS, then were incubated with 90 μl of the fresh culture medium and 10 μl (5 mg/ml) of MTT (3-[4,5-dimethylthiazol-2-yl]-2,5-diphenyltetrazolium bromide) for 4 hr. Finally, MTT formazan crystals were dissolved in the medium by adding 200 μl dimethyl sulfoxide (DMSO). After that, the plate was placed on the orbital shaker for 20 min. The optical density (OD) was measured at 570 nm using a multiwall spectrophotometer (ELISA reader (Stat Fax 3200, Awareness Technology, USA)). The viability (%) of cells in different groups was calculated according to the following formula:

$$\text{Viability} = (\text{mean OD570 nm of the treated group/mean OD570 nm of the control group}) \times 100\%.$$

2.5. Irradiation. The cells were irradiated with megavoltage X-ray (6 MV) using Elekta Compact linear accelerator (Emam Reza Hospital, Mashhad, Iran) at a dose rate of 3 Gy/min with a field size of $20 \times 20\ \text{cm}^2$. In this study, we used five plexiglass (water equivalent) sheets with 1.5 cm thickness placed under the bottom of the plate to sufficiently production of backscatter.

2.6. Colony Formation Assay. The radiosensitivity caused by the presence of nanoparticles was assessed in MCF-7 cells by colony formation assay test. The colony-forming assay is the gold standard for measuring radiosensitivity. An appropriate number of MCF-7 cells (400, 1,000, 1,200, 1,400 for irradiation doses of 0, 2, 4, and 6 Gy, respectively) were seeded in 6-well plates and incubated in RPMI 1640 medium containing 10% FBS and 1% penicillin-streptomycin at 37°C in 5% CO_2 atmosphere 24 hr before treatment to allow attachment. Plates were divided into three groups: in the first group (without nanoparticles) medium was replaced with 3 ml of fresh medium. Second, the culture medium was replaced with fresh media containing Bi_2S_3@BSA at a concentration of 75 μg/ml. In the third group, the culture medium was replaced with the fresh media at a concentration of 75 μg/ml of Bi_2S_3@BSA-triptorelin, then incubated for 24 hr. Next, the medium inside each well of all plates was removed. The cells were washed twice with PBS, and 3 cc fresh culture medium (10% FBS) was added into each well. Then, the cells were exposed to radiation doses of 0, 2, 4, 6 Gy irradiated with 6 MV photon beams (Elekta Compact linear accelerator). Immediately after irradiation, the cells were incubated (10% FBS and 1% penicillin−streptomycin at 37°C in 5% CO_2) for ten days to allow colony formation. During this time, the medium was added to the plates as needed.

The colonies were fixed with methanol and acetic acid (3 : 1). Performed Giemsa staining after 24 hr. The colonies exceeding 50 cells were counted. The survival fraction (SF) was calculated using the following formula:

$$\text{SF} = \frac{\text{Number of colonies counted}}{\text{Number of cells cultured} \times \text{PE}/100}, \quad (1)$$

where

$$\text{PE (plate efficiency)} = \frac{\text{Number of colonies counted}}{\text{Number of cells cultured without any treatment}} \times 100. \quad (2)$$

The data fitted to the linear-quadratic model with the equation of SF = exp $(-\alpha D - \beta D2)$ and the survival curve were estimated using GraphPad Prism2018 software. In addition, α and β parameters of the survival curve were calculated with GraphPad Prism2018 software.

2.7. Apoptosis by Annexin-V FITC Assay. The two major mechanisms of cell death are apoptosis and necrosis. To determine the rate of apoptosis and quantify the number of apoptotic cells, flow cytometry (annexin V) was used. MCF-7 cells were cultured in 6-well plates at a density of 5,00,000 cells per well. Then were incubated (24 hr) in an RPMI 1640 medium containing 10% FBS and 1% penicillin–streptomycin at 37°C in a 5% CO_2 atmosphere. Briefly, the cells were treated with free nanoparticles, Bi_2S_3@BSA (75 μg/ml), and Bi_2S_3@BSA–triptorelin (75 μg/ml) for 24 hr. The culture medium of all wells of plates was removed. The cells were washed twice with PBS, and 3 cc fresh culture medium (10% FBS) was added to each well. Then, the cells were exposed to radiation doses of 0, 2, 4, 6 Gy with 6 MV photon beams (Elekta Compact linear accelerator). After 24 hr, the cells were trypsinized and washed twice in PBS. After that, the harvested cells were collected by centrifugation at 1,500 rpm for 3 min, then resuspended in 0.5 ml binding buffer. The cell suspension was incubated with 7 μl annexin V-FITC for 15 min and 5 μl PI for 5 min at room temperature in the dark. Finally, the samples (stained cells) were analyzed immediately with flow cytometry (BD Accuri C6). Quantification of results was performed using Flowjo 7.6 software. Viable cells were identified with negative cells of annexin V-FITC and PI; early apoptotic cells were identified with annexin V-FITC positive cells; late apoptotic cells were identified with positive annexin V-FITC and PI cells; finally, to determine necrotic cells, positive PI and negative annexin cells were considered.

2.8. Statistical Analysis. GraphPad Prism2018 software was used to perform statistical analysis. Differences in percentage cell viability between groups were analyzed by one-way ANOVA and Tukey's multiple comparison tests ($P < 0.05$). All graphs were plotted by using GraphPad Prism2018 software.

3. Result

3.1. Characteristics. Figure 2(a) shows the transmission electron microscopy (TEM) image of Bi_2S_3@BSA NPs. The morphology of Bi_2S_3@BSA NPs was spherical. The average size was 8.649 ± 1.69 nm. Figure 2(b)–2(g) shows the size distribution and zeta potential of Bi_2S_3@BSA and Bi_2S_3@BSA–triptorelin NPs. The average sizes of Bi_2S_3@BSA and Bi_2S_3@BSA–triptorelin NPs were about 16 ± 2 nm and 17.1 ± 2 nm, with a zeta potential of -77.8 ± 3.80 mV and -84.7 ± 2.18 mV. The poly index of Bi_2S_3@BSA was 0.623 ± 0.033. The average size of Bi_2S_3 NPs was 14.2 nm with a zeta potential of -69.8 ± 2.90 mV. Moreover, the results showed that the hydrodynamic size of Bi_2S_3@BSA–triptorelin NPs after 24 hr incubation was 17.3 ± 1.1 nm, which showed good stability in the cellular environment. All diffraction peaks of Bi_2S_3@BSA NPs almost demonstrated the Bi_2S_3 structure (JCPDS No. 43-1471) [30]. According to the XRD (X-ray powder diffraction) pattern, all the peaks were well indexed to the orthorhombic Bi_2S_3 crystal (Figure 3(a)) because Bi_2S_3 NPs coated with BSA, Bi_2S_3@BSA NPs are not exactly in agreement with the standard card (peak in the areas of 20°–30° is related to the BSA) [31]. To confirm the conjugation of triptorelin on the surface of Bi_2S_3@BSA NPs, FT-IR spectroscopy was done. Figure 3(b) shows the FT-IR spectrum of functionalized Bi_2S_3@BSA and Bi_2S_3@BSA–triptorelin NPs. The formation of peaks 1,651 and 1,576 cm^{-1} is related to primary and secondary amide and amine bonds. It shows the presence of BSA on the nanoparticle surface. The removal of the thiol peak at 2,360 cm^{-1} is due to the presence of a complex between bismuth and thiol, which leads to the formation of a bismuth–sulfur bond; finally, a sulfide bond is obtained. Peak 670 cm^{-1} could also be related to bismuth sulfide bonding. The peptide binds to the nanoparticle surface via an amide bond. Due to the presence of BSA on the nanoparticle surface, amide bonds appeared together in 1,663 cm^{-1} because of the new amid bonds that were in accordance with redshift. Peak 1,651 cm^{-1}, which corresponds to the BSA amide peak, disappeared and changed to peak 1,633 cm^{-1} due to the amide bond between triptorelin and BSA. The presence of peak 702 cm^{-1} indicates the bonding of aromatic hydrocarbon, which is related to the aromatic ring of the triptorelin peptide compound.

3.2. In Vitro Cytotoxicity Assay. The cytotoxicity of NPs was measured by the MCF-7 cell line. The MCF-7 cell line was treated with Bi_2S_3@BSA NPs, Bi_2S_3@BSA–triptorelin NPs at different concentrations (0, 5, 10, 15, 25, 50, 100, 150, and 200 μg/ml) for 24 hr. Figure 4 shows the percentage cell viability of the MCF-7 cell lines incubated with NPs at different concentrations.

The results of the MTT test presented the viability of cells incubated with Bi_2S_3@BSA and Bi_2S_3@BSA–triptorelin at different concentrations. There were no significant differences (not toxic) between the control and test groups ($P < 0.05$) up to 150 and 75 μg/ml, respectively. Since the purpose of this study was to use Bi_2S_3@BSA as a radiosensitizer with low toxicity, concentrations of 75 μg/ml were used for colony and apoptosis assay.

3.3. In Vitro Radiosensivity Assay. In order to investigate the effect of nanoparticles as a radiosensitizer, colony formation

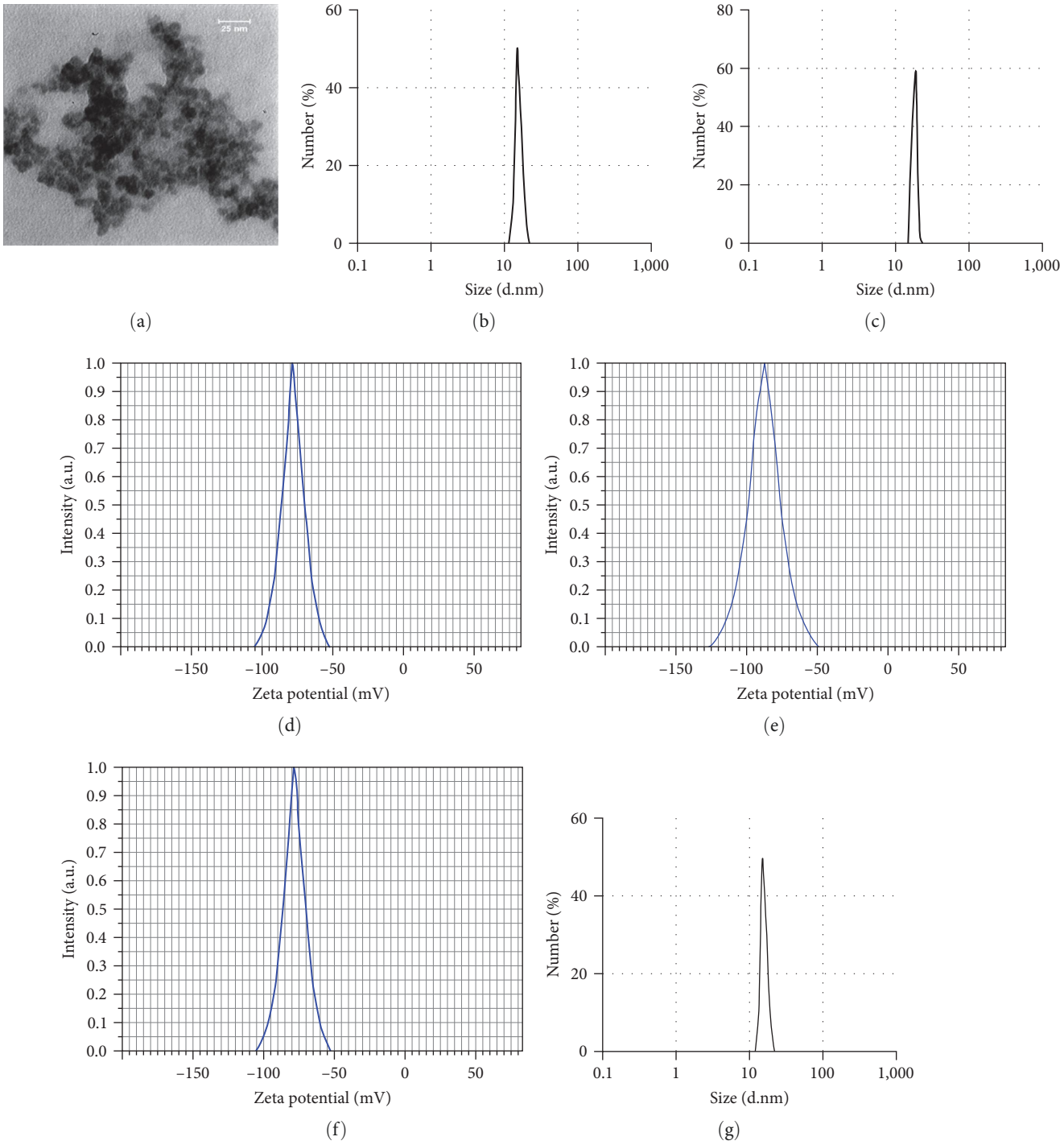

FIGURE 2: (a) TEM image of Bi_2S_3@BSA NPs, (b) and (c) size distribution and (d) and (e) zeta potential of Bi_2S_3@BSA NPs and Bi_2S_3@BSA–triptorelin NPs, (f) and (g) shows zeta potential and size distribution of Bi_2S_3 NPs.

assay as the "Gold Standard" of radiosensitivity was performed, and the survival curve was plotted (Figure 5 (vertical axis at logarithmic scale)). The results showed that a nontoxic concentration of nanoparticles (75 μg/ml) at RT reduced the viability of MCF7 cells. The viability of cells treated with Bi_2S_3@BSA–triptorelin, Bi_2S_3@BSA, and cells that were not treated with nanoparticles at all doses was significantly decreased ($P<0.05$). SFs for groups of cells not treated with nanoparticles and were just exposed to radiation doses 2, 4, and 6 Gy, also radiation as well as triptorelin (irradiated with 6 MV photon beams), were 79.49%, 54.21%, 22.24%, and 79.1%, 54.6%, 21.9%, respectively. There was no difference between the groups of cells treated with radiation alone and radiation plus triptorelin ($P<0.05$). In the presence of Bi_2S_3@BSA (75 μg/ml), they were 53%, 31%, and 12%, respectively, and decreased to 35%, 12.5%, and 2% in the

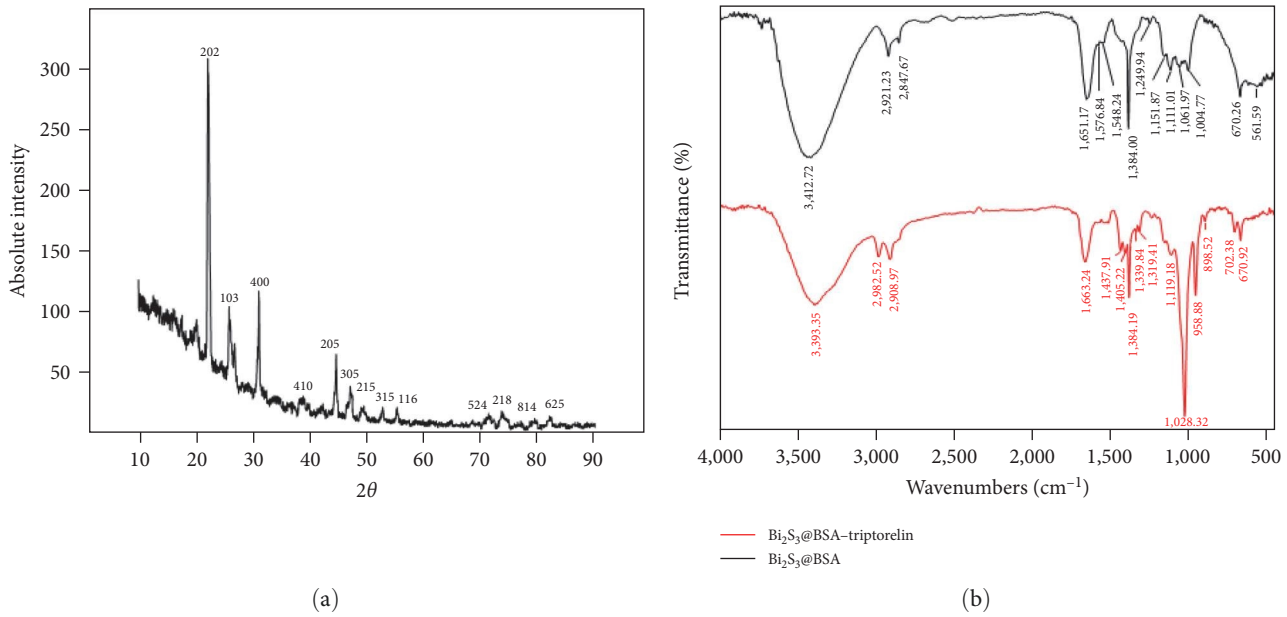

FIGURE 3: (a) X-ray diffraction pattern of Bi_2S_3@BSA, (b) Fourier transform infrared spectra of Bi_2S_3@BSA NPs, Bi_2S_3@BSA–triptorelin.

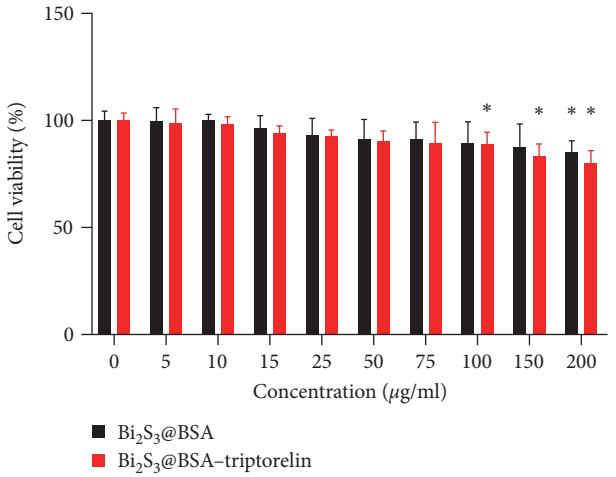

FIGURE 4: Percentage cell viability of the MCF-7 cells incubated with different concentrations of Bi_2S_3@BSA NPs and Bi_2S_3@BSA–triptorelin NPs. Error bars indicate the standard error of the mean (SEM) for $n = 3$ independent experiments. *Indicates significant difference with $P < 0.05$.

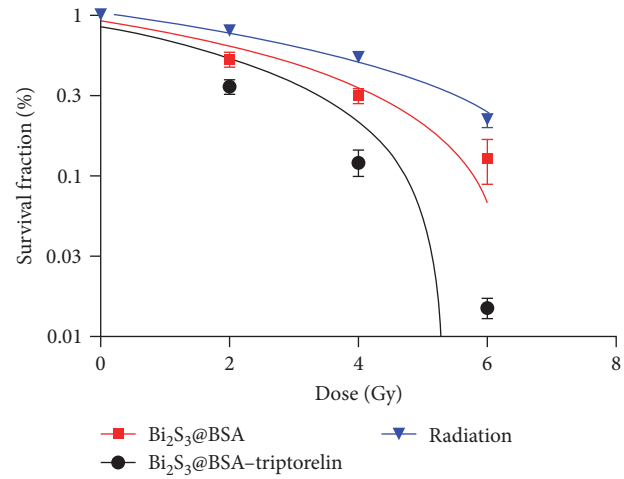

FIGURE 5: Survival curves of MCF-7 cells with 75 μg/ml concentrations of Bi_2S_3@BSA NPs and Bi_2S_3@BSA–triptorelin NPs irradiated with 6 MV. Error bars indicate the standard error of the mean (SEM) for $n = 3$ independent experiments.

presence of Bi_2S_3@BSA–triptorelin. Table 1 shows α and β parameters of the survival curve for different groups.

3.4. Effects of NPs on MCF-7 Cell Apoptosis. In the current study, to investigate the mechanism of nanoparticle radiosensitivity, annexin V-FITC/PI staining was used. The result indicated that when cells were treated with Bi_2S_3@BSA–triptorelin (75 μg/ml) of nanoparticles in combination with radiation, apoptotic percentage induced in the MCF-7 cells was significantly higher compared to cells treated with Bi_2S_3@BSA and radiation ($P < 0.05$). In addition, MCF-7 cells treated with Bi_2S_3@BSA and exposed to 6 MV irradiation induced a significant increase in apoptosis compared to MCF-7 cells irradiated alone. There was no difference between the groups of cells treated with radiation alone and radiation plus triptorelin ($P < 0.05$). Figures 6 and 7 show the result of flow cytometry. Percentages of necrotic cells were not significantly different among the cells treated with targeted and nontargeted nanoparticles in combination with RT or those treated with radiation alone.

4. Discussion

It is usually suggested that one crucial factor that affects cytotoxicity is nanoparticle size. Smaller nanoparticles have a larger surface-area-to-volume ratio and could decrease cell

Table 1: Values of α, β ($\pm$SD) of MCF-7 cells in different groups.

Groups	α (Gy^{-1})	β (Gy^{-2})
Radiation	0.08626 ± 0.01019	0.007169 ± 0.001628
Radiation + Bi_2S_3@BSA	0.2226 ± 0.02893	0.01284 ± 0.004621
Radiation + Bi_2S_3@BSA–triptorelin	0.3623 ± 0.01442	0.03375 ± 0.002304

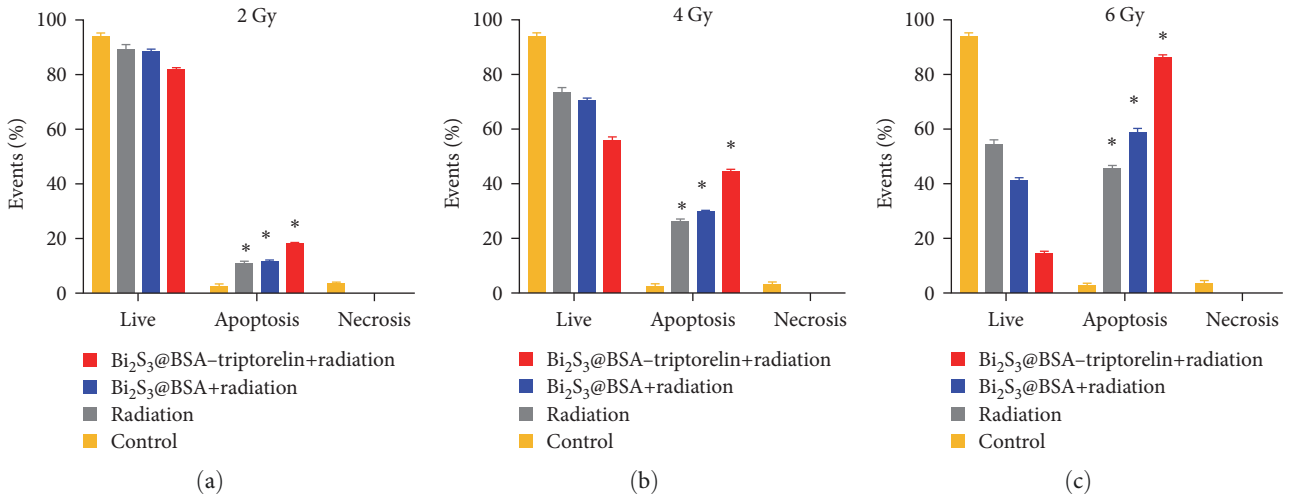

Figure 6: Percentage (%) of living, apoptotic, and necrotic in MCF-7 cells treated or not treated with Bi_2S_3@BSA NPs and Bi_2S_3@BSA–triptorelin induced after (a) 2 Gy, (b) 4 Gy, and (c) 6 Gy radiation doses and control (no any treatment. Error bars indicate the standard error of the mean (SEM) for $n = 3$ independent experiments. *indicates significant difference with $P < 0.05$.

viability. Many studies also show that the cytotoxicity of several types of nanoparticles was size-dependent [32]. A study by Algethami et al. [33] investigated the toxicity of Bi_2S_3 (PVP coated) nanoparticles with a diameter of 3–5 nm on PC3 cell lines for 48hr. Even at concentrations of 0.5 mM, the nanoparticles are not toxic. Our results show that in MCF-7 cells treated with different concentrations of Bi_2S_3@BSA, no significant toxicity was observed, even up to 150 μg/ml concentration. This difference could be due to the surface coating of the nanoparticles and the type of cell line used for the experiment. In the study of Azizi et al. [34], the cytotoxicity of Bi_2S_3@BSA nanoparticles with a hydrodynamic size of 107.6 ± 6.81 nm on 4T1 cell lines was evaluated, and the viability of the 4T1 cells treated with Bi_2S_3@BSA (200 μg/ml) nanoparticles was significantly reduced, which almost follow the results of our study. In addition, there are no appropriate studies to compare the biocompatibility of nanoparticles in this study, as the toxicity of Bi-based compounds varies with cell lines and concentrations. Also, other studies have shown that BSA improves the biocompatibility of Bi_2S_3 nanoparticles [35–37].

The radiosensitivity effect of nanoparticles in combination with high energy is suggested in nanoparticle-treated cells [38, 39]. Recently, bismuth-based nanomaterials have demonstrated their ability to increase radiation dose, their application in multimodal imaging, their ability to act as computed tomography (CT) contrast agents, and their biocompatibility [40]. The results of this study demonstrate that Bi_2S_3@BSA increases the radiosensitivity of MCF-7 cells at all doses using low linear energy transfer. Our results are consistent with Ma et al.'s [41] study, which treated PC3 cells with Bi_2S_3-embedded mesoporous silica nanoparticles and investigated the radiosensitizing effects of these nanoparticles in radionuclide combination therapy (P-32). They suggested that the inhibition rate of the cell group treated with P-32 treatment was only 16.1% (24 hr), whereas the inhibition rate after treatment with nanoparticles (50 μg/ml) and RT was 57% (24 hr), which was significantly enhanced. These results are supported by Huang et al. [42]. They reported less than 20% cell inhibition (after 48 hr) in the PC3 cell line (P-32) treated with radiation. While Bi_2S_3-PLGA capsules (200 μg/ml) and irradiation (P-32) resulted in greater than 30% cell inhibition. Finally, declared that cell inhibition is a concentration-dependent cell inhibition in the PC3 cell lines. Apart from that, Azizi et al. [34] observed that Bi_2S_3@BSA nanoparticles as radiosensitizers increased the sensitivity of cancer cells to radiation. Given the radiosensitivity effects of Bi_2S_3 nanoparticles at megavoltage energies, there is a report published by Abhari et al. [43]. They reported that increasing concentrations of Bi_2S_3-BSA enhanced the inhibition of cell proliferation (4T1). Other studies on the use of Bi_2S_3 nanoparticles in RT have been limited to kilovoltage energies. This study may provide researchers with useful data in the field of radiosensitivity of bismuth-based nanoparticles at megavoltage energies.

This in vitro study demonstrated that nontoxic concentrations of bovine serum albumin-coated Bi_2S_3 nanoparticles significantly ($P < 0.05$) induced radiosensitivity in the MCF-7 cell line when exposed to MV X-rays at all doses. These

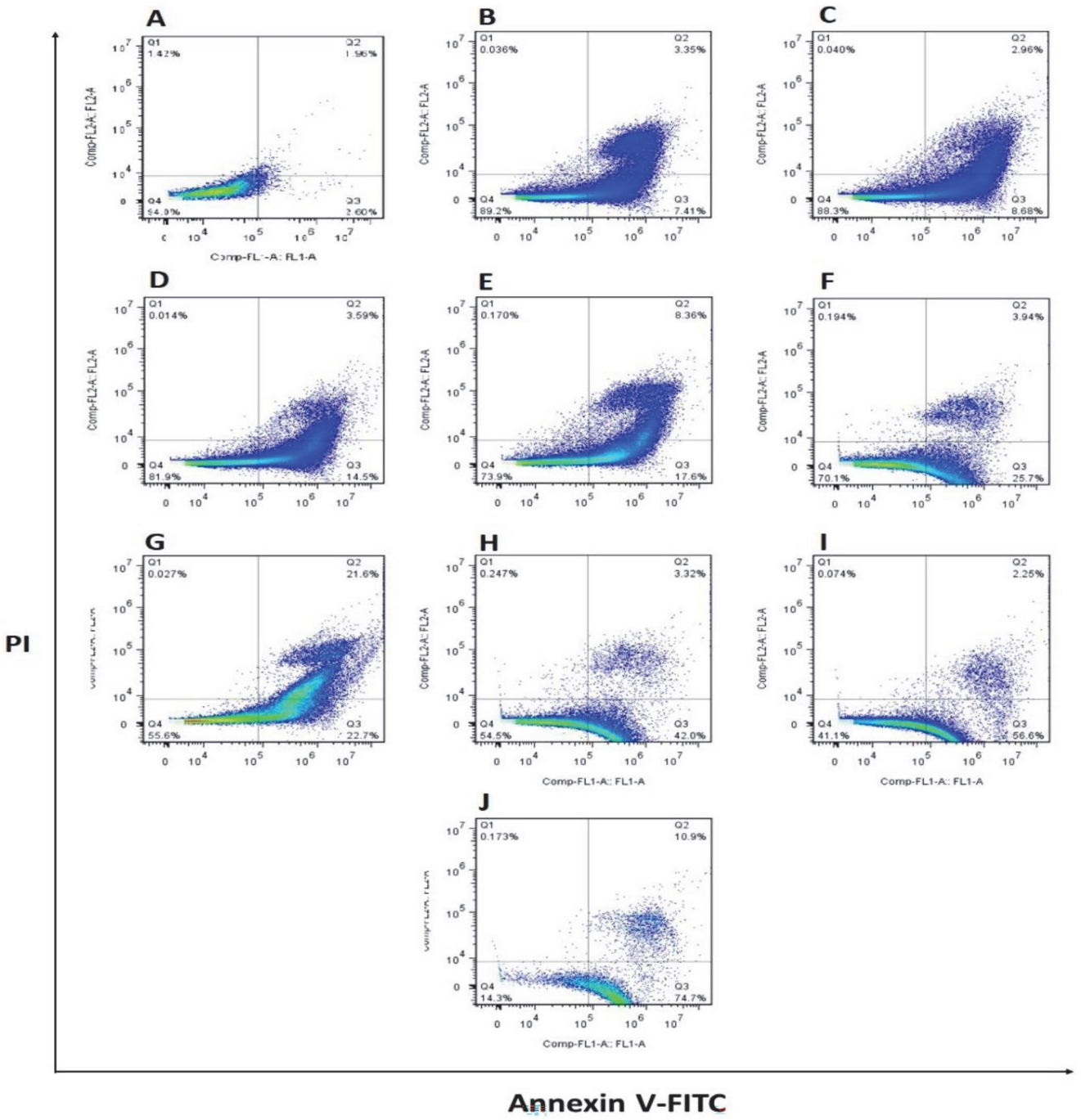

Figure 7: Flow cytometry analysis of apoptosis in MCF-7 cells stained with annexin V-FITC and PI: (a) control (no treatment), (b) X-ray alone (2 Gy), (c) X-ray (2 Gy) + Bi_2S_3@BSA, (d) X-ray (2 Gy) + Bi_2S_3@BSA–triptorelin, (e) X-ray alone (4 Gy), (f) X-ray (4 Gy) + Bi_2S_3@BSA, (g) X-ray (4 Gy) + Bi_2S_3@BSA–triptorelin, (h) X-ray alone (6 Gy), (i) X-ray (6 Gy) + Bi_2S_3@BSA, (j) X-ray (6 Gy) + Bi_2S_3@BSA–triptorelin.

results are fully consistent with the study by Abhari et al. [43]. The study conducted by Ai et al. [44] suggested that Bi_2S_3 NPs are internalized into cells via endocytosis. This enhancement in radiosensitivity can be attributed to the fact that the internalized NPs in target cells in interaction with ionization radiation may produce high numbers of free radicals through photoelectric and Compton interactions. These additional free radicals would increase the probability of DNA damage and subsequent cell death, thus enhancing the radiosensitivity [33]. The surviving fractions of MCF-7 cells were determined to assess the radiosensitization effect of nanoparticles. Colony formation assay results showed significantly lower viability of MCF-7 cells treated with Bi_2S_3@BSA-triptorelin nanoparticles + X-rays at all doses compared to Bi_2S_3@BSA nanoparticles + X-rays ($P < 0.05$). Also, the decrease in viability of targeted and nontargeted

nanoparticles was dependent on the X-ray exposure dose. Maybe the triptorelin conjugated with Bi_2S_3@BSA could enhance the internalization of Bi_2S_3@BSA nanoparticles through the GnRH receptors in MCF-7 cells. A parallel study by Mohammadi et al. [45] was performed on bismuth sulfide nanoparticles coated with BSA and targeted with a triptorelin peptide (nanoparticles similar to this study). CT imaging was used to identify differences in MCF-7 cellular uptake between targeted and nontargeted nanoparticles at 75 μg/ml concentration at 90 kVp; the X-ray attenuation intensity of cells in the presence of targeted nanoparticles is 1.4 times greater than cells in the presence of nontargeted nanoparticles, which indicates an increase in the uptake of targeted nanoparticles by MCF-7 cells.

Zoghi et al. [46] showed that the biodistribution of a tracer targeted by triptorelin showed significant uptake in tumors expressing GnRH receptors. The results of our study in this section are consistent with those obtained by Yu et al. [47]. Their results showed Bi-NPs exhibited higher tumor accumulation after binding with the tumor-homing peptide LyP-1. BiLyP-1 NPs exhibited a significant radiosensitizing effect in interaction with ionizing radiation (because of more internalization into cells). Also, our results are in agreement with the Obayemi et al. [48] report, which demonstrated that LHRH-conjugated nanoparticles specifically bind to receptors overexpressed on the surface of most breast cancer cell types.

After treatment, the flow cytometry analyses on MCF-7 cells were performed to investigate the possible mechanism of radiosensitivity. Our results (Figures 6 and 7) showed that the amount of apoptosis was significantly higher than that of necrosis in all groups. This observation may introduce apoptosis as the major mechanism that determines radiosensitivity. Our results were consistent with those obtained by Ma et al. [41]. They introduced apoptosis as mainly contributing to the antiproliferative effects of Bi_2S_3-embedded mesoporous silica nanoparticles in combination with P-32 radiation. Li et al. [49] suggested that in 4T1 cells treated with Fe@Bi_2S_3 + radiation, apoptosis more than necrosis induces cell death, which is consistent with our results. In our study, targeted nanoparticles compared to nontargeted induced significantly more apoptosis nanoparticles ($P<0.05$), which confirmed the colony formation assay results. In this study, we observed an increase in radiosensitization by targeted nanoparticles. It can be inferred that apoptosis was related to the radiosensitivity and cell death induced by nanoparticles plus radiation. More studies are needed to specify the role of nanoparticles in biological pathways affecting apoptosis and other biological interactions.

5. Conclusion

For the first time, novel targets based on Bi_2S_3@BSA and triptorelin were developed using an inexpensive functionalization process with a spherical shape, small size, and appropriate zeta potential to improve quality and reduce breast cancer radiotherapy side effects. In this study, we have successfully improved the stability of Bi_2S_3 nanoparticles by using BSA because of its chemical stability and nontoxicity. Bi_2S_3@BSA conjugated with triptorelin can target the GnRH receptors expressed on breast cancer cells membrane. The toxic effect of Bi_2S_3@BSA nanoparticles conjugated with triptorelin on the MCF-7 cell lines under megavoltage X-ray radiation demonstrated that Bi_2S_3@BSA–triptorelin nanoparticles, as a targeted radiosensitizer, increased the radiosensitivity of breast cancer cells. These properties of nanoparticles have raised the possibility of using them as a promising candidate for in vitro and in vivo (in future studies) therapeutic experiments aimed at developing and achieving cancer medication for cancer therapy.

Data Availability

The data presented in this study are available on request from the corresponding authors.

Conflicts of Interest

The authors declare that they have no conflicts of interest.

Funding

This article is based on the results exploited from an M.Sc. thesis (Code: 971956) that is supported by the Medical Physics Department of Mashhad University of Medical Sciences.

Acknowledgments

The authors would like to thank all members of the Medical Physics Department of Mashhad University of Medical Sciences.

References

[1] R. Bazak, M. Houri, S. El Achy, W. Hussein, and T. Refaat, "Passive targeting of nanoparticles to cancer: a comprehensive review of the literature," *Molecular and Clinical Oncology*, vol. 2, no. 6, pp. 904–908, 2014.

[2] M. M. Fathy, F. S. Mohamed, N. S. Elbialy, and W. M. Elshemey, "Multifunctional chitosan-capped gold nanoparticles for enhanced cancer chemo-radiotherapy: an invitro study," *Physica Medica*, vol. 48, pp. 76–83, 2018.

[3] A. Rajaee, S. Wang, L. Zhao et al., "Multifunction bismuth gadolinium oxide nanoparticles as radiosensitizer in radiation therapy and imaging," *Physics in Medicine & Biology*, vol. 64, Article ID 195007, 2019.

[4] L. Cui, S. Her, G. R. Borst, R. G. Bristow, D. A. Jaffray, and C. Allen, "Radiosensitization by gold nanoparticles: will they ever make it to the clinic?" *Radiotherapy and Oncology*, vol. 124, no. 3, pp. 344–356, 2017.

[5] Z. Rezaee, A. Yadollahpour, V. Bayati, and F. N. Dehbashi, "Gold nanoparticles and electroporation impose both separate and synergistic radiosensitizing effects in HT-29 tumor cells: an in vitro study," *International Journal of Nanomedicine*, vol. 12, pp. 1431–1439, 2017.

[6] J. Deng, S. Xu, W. Hu, X. Xun, L. Zheng, and M. Su, "Tumor targeted, stealthy and degradable bismuth nanoparticles for enhanced X-ray radiation therapy of breast cancer," *Biomaterials*, vol. 154, pp. 24–33, 2018.

[7] J. F. Hainfeld, F. Avraham Dilmanian, D. N. Slatkin, and H. M. Smilowitz, "Radiotherapy enhancement with gold nanoparticles," *Journal of Pharmacy and Pharmacology*, vol. 60, no. 8, pp. 977–985, 2008.

[8] G. Gordon Steel and M. J. Peckham, "Exploitable mechanisms in combined radiotherapy-chemotherapy: the concept of additivity," *International Journal of Radiation Oncology Biology Physics*, vol. 5, no. 1, pp. 85–91, 1979.

[9] T. Cardilin, J. Almquist, M. Jirstrand, A. Zimmermann, S. El Bawab, and J. Gabrielsson, "Model-based evaluation of radiation and radiosensitizing agents in oncology," *CPT: Pharmacometrics & Systems Pharmacology*, vol. 7, no. 1, pp. 51–58, 2018.

[10] M.-T. Bahreyni-Toossi, E. Dolat, H. Khanbabaei, N. Zafari, and H. Azimian, "microRNAs: potential glioblastoma radiosensitizer by targeting radiation-related molecular pathways," *Mutation Research/Fundamental and Molecular Mechanisms of Mutagenesis*, vol. 816-818, Article ID 111679, 2019.

[11] P. Wardman, "Chemical radiosensitizers for use in radiotherapy," *Clinical Oncology*, vol. 19, no. 6, pp. 397–417, 2007.

[12] A.-L. Papa, S. Basu, P. Sengupta, D. Banerjee, S. Sengupta, and R. Harfouche, "Mechanistic studies of gemcitabine-loaded nanoplatforms in resistant pancreatic cancer cells," *BMC Cancer*, vol. 12, Article ID 419, 2012.

[13] J. Xie, L. Gong, S. Zhu, Y. Yong, Z. Gu, and Y. Zhao, "Emerging strategies of nanomaterial-mediated tumor radiosensitization," *Advanced Materials*, vol. 31, no. 3, Article ID 1802244, 2019.

[14] C. Stewart, K. Konstantinov, S. McKinnon et al., "First proof of bismuth oxide nanoparticles as efficient radiosensitisers on highly radioresistant cancer cells," *Physica Medica*, vol. 32, no. 11, pp. 1444–1452, 2016.

[15] R. Zhou, X. Liu, Y. Wu et al., "Suppressing the radiation-induced corrosion of bismuth nanoparticles for enhanced synergistic cancer radiophototherapy," *ACS Nano*, vol. 14, no. 10, pp. 13016–13029, 2020.

[16] L. Jiao, Q. Li, J. Deng, N. Okosi, J. Xia, and M. Su, "Nanocellulose templated growth of ultra-small bismuth nanoparticles for enhanced radiation therapy," *Nanoscale*, vol. 10, no. 14, pp. 6751–6757, 2018.

[17] A. L. Brown and A. M. Goforth, "pH-dependent synthesis and stability of aqueous, elemental bismuth glyconanoparticle colloids: potentially biocompatible X-ray contrast agents," *Chemistry of Materials*, vol. 24, no. 9, pp. 1599–1605, 2012.

[18] M. Hossain and M. Su, "Nanoparticle location and material-dependent dose enhancement in X-ray radiation therapy," *The Journal of Physical Chemistry C*, vol. 116, no. 43, pp. 23047–23052, 2012.

[19] X.-D. Zhang, Z. Luo, J. Chen et al., "Ultrasmall $Au_{10-12}(SG)_{10-12}$ nanomolecules for high tumor specificity and cancer radiotherapy," *Advanced Materials*, vol. 26, no. 26, pp. 4565–4568, 2014.

[20] A. V. Schally and A. Nagy, "Chemotherapy targeted to cancers through tumoral hormone receptors," *Trends in Endocrinology & Metabolism*, vol. 15, no. 7, pp. 300–310, 2004.

[21] Ž. Krpetić, S. Anguissola, D. Garry, P. M. Kelly, and K. A. Dawson, "Nanomaterials: impact on cells and cell organelles," in *Nanomaterial*, D. Capco and Y. Chen, Eds., vol. 811 of *Advances in Experimental Medicine and Biology*, pp. 135–156, Springer, Dordrecht, 2014.

[22] E. Mahon, A. Salvati, F. B. Bombelli, I. Lynch, and K. A. Dawson, "Designing the nanoparticle–biomolecule interface for "targeting and therapeutic delivery"," *Journal of Controlled Release*, vol. 161, no. 2, pp. 164–174, 2012.

[23] R. C. Ladner, A. K. Sato, J. Gorzelany, and M. de Souza, "Phage display-derived peptides as therapeutic alternatives to antibodies," *Drug Discovery Today*, vol. 9, no. 12, pp. 525–529, 2004.

[24] S. M. P. Vadevoo, S. Gurung, F. Khan et al., "Peptide-based targeted therapeutics and apoptosis imaging probes for cancer therapy," *Archives of Pharmacal Research*, vol. 42, pp. 150–158, 2019.

[25] N. Zhao, Z. Yang, B. Li et al., "RGD-conjugated mesoporous silica-encapsulated gold nanorods enhance the sensitization of triple-negative breast cancer to megavoltage radiation therapy," *International Journal of Nanomedicine*, vol. 11, pp. 5595–5610, 2016.

[26] X. Deng, Q. Qiu, K. Ma, W. Huang, and H. Qian, "Synthesis and in vitro anti-cancer evaluation of luteinizing hormone-releasing hormone-conjugated peptide," *Amino Acids*, vol. 47, pp. 2359–2366, 2015.

[27] A. R. Günthert, C. Gründker, A. Olota, J. Läsche, N. Eicke, and G. Emons, "Analogs of GnRH-I and GnRH-II inhibit epidermal growth factor-induced signal transduction and resensitize resistant human breast cancer cells to 4OH-tamoxifen," *European Journal of Endocrinology*, vol. 153, no. 4, pp. 613–625, 2005.

[28] M. Fekete, J. L. Wittliff, and A. V. Schally, "Characteristics and distribution of receptors for [d-trp^6]-luteinizing hormone-releasing hormone, somatostatin, epidermal growth factor, and sex steroids in 500 biopsy samples of human breast cancer," *Journal of Clinical Laboratory Analysis*, vol. 3, no. 3, pp. 137–147, 1989.

[29] R. Wahab, M. A. Siddiqui, Q. Saquib et al., "ZnO nanoparticles induced oxidative stress and apoptosis in HepG2 and MCF-7 cancer cells and their antibacterial activity," *Colloids and Surfaces B: Biointerfaces*, vol. 117, pp. 267–276, 2014.

[30] Y. Wang, Y. Wu, Y. Liu et al., "BSA-mediated synthesis of bismuth sulfide nanotheranostic agents for tumor multimodal imaging and thermoradiotherapy," *Advanced Functional Materials*, vol. 26, no. 29, pp. 5335–5344, 2016.

[31] P. Yang, Q. Liu, J. Liu et al., "Bovine serum albumin-coated graphene oxide for effective adsorption of uranium (VI) from aqueous solutions," *Industrial & Engineering Chemistry Research*, vol. 56, no. 13, pp. 3588–3598, 2017.

[32] N. N. T. Sisin, S. Z. Abidin, M. A. Yunus, H. M. Zin, K. A. Razak, and W. N. Rahman, "Evaluation of bismuth oxide nanoparticles as radiosensitizer for megavoltage radiotherapy," *International Journal on Advanced Science, Engineering and Information Technology*, vol. 9, no. 4, pp. 1434–1443, 2019.

[33] M. Algethami, M. Geso, T. Piva et al., "Radiation dose enhancement using Bi_2S_3 nanoparticles in cultured mouse PC3 prostate and B16 melanoma cells," *NanoWorld Journal*, vol. 1, no. 2, 2015.

[34] S. Azizi, H. Nosrati, A. Sharafi, and H. Danafar, "Preparation of bismuth sulfide nanoparticles as targeted biocompatible nano-radiosensitizer and carrier of methotrexate," *Applied Organometallic Chemistry*, vol. 34, no. 1, Article ID e5251, 2020.

[35] M. H. Faghfoori, H. Nosrati, H. Rezaeejam et al., "Anticancer effect of X-Ray triggered methotrexate conjugated albumin coated bismuth sulfide nanoparticles on SW480 colon cancer cell line," *International Journal of Pharmaceutics*, vol. 582, Article ID 119320, 2020.

[36] H. Nosrati, F. Abhari, J. Charmi et al., "Facile green synthesis of bismuth sulfide radiosensitizer *via* biomineralization of albumin natural molecule for chemoradiation therapy aim,"

Artificial Cells, Nanomedicine, and Biotechnology, vol. 47, no. 1, pp. 3832–3838, 2019.

[37] H. Nosrati, E. Attari, F. Abhari et al., "Complete ablation of tumors using synchronous chemoradiation with bimetallic theranostic nanoparticles," *Bioactive Materials*, vol. 7, pp. 74–84, 2022.

[38] F. Geng, K. Song, J. Z. Xing et al., "Thio-glucose bound gold nanoparticles enhance radio-cytotoxic targeting of ovarian cancer," *Nanotechnology*, vol. 22, no. 28, Article ID 285101, 2011.

[39] C. Wang, X. Li, Y. Wang, Z. Liu, L. Fu, and L. Hu, "Enhancement of radiation effect and increase of apoptosis in lung cancer cells by thio-glucose-bound gold nanoparticles at megavoltage radiation energies," *Journal of Nanoparticle Research*, vol. 15, Article ID 1642, 2013.

[40] X. Cheng, Y. Yong, Y. Dai et al., "Enhanced radiotherapy using bismuth sulfide nanoagents combined with photothermal treatment," *Theranostics*, vol. 7, no. 17, pp. 4087–4098, 2017.

[41] M. Ma, Y. Huang, H. Chen et al., "Bi_2S_3-embedded mesoporous silica nanoparticles for efficient drug delivery and interstitial radiotherapy sensitization," *Biomaterials*, vol. 37, pp. 447–455, 2015.

[42] Y. Huang, M. Ma, S. Chen, J. Dai, F. Chen, and Z. Wang, "Construction of multifunctional organic–inorganic hybrid Bi_2S_3-PLGA capsules for highly efficient ultrasound-guided radiosensitization of brachytherapy," *RSC Advances*, vol. 4, no. 51, pp. 26861–26865, 2014.

[43] F. Abhari, J. Charmi, H. Rezaeejam et al., "Folic acid modified bismuth sulfide and gold heterodimers for enhancing radiosensitization of mice tumors to X-ray radiation," *ACS Sustainable Chemistry & Engineering*, vol. 8, no. 13, pp. 5260–5269, 2020.

[44] K. Ai, Y. Liu, J. Liu, Q. Yuan, Y. He, and L. Lu, "Large-scale synthesis of Bi_2S_3 nanodots as a contrast agent for in vivo X-ray computed tomography imaging," *Advanced Materials*, vol. 23, no. 42, pp. 4886–4891, 2011.

[45] M. Mohammadi, S. Khademi, Y. Choghazrdi, R. Irajirad, M. Keshtkar, and A. Montazerabadi, "Modified bismuth nanoparticles: a new targeted nanoprobe for computed tomography imaging of cancer," *Cell Journal (Yakhteh)*, vol. 24, no. 9, pp. 515–521, 2022.

[46] M. Zoghi, A. R. Jalilian, A. Niazi, F. Johari-Daha, B. Alirezapour, and S. Ramezanpour, "Development of a ^{68}Ga-peptide tracer for PET GnRH1-imaging," *Annals of Nuclear Medicine*, vol. 30, pp. 400–408, 2016.

[47] X. Yu, A. Li, C. Zhao, K. Yang, X. Chen, and W. Li, "Ultrasmall semimetal nanoparticles of bismuth for dual-modal computed tomography/photoacoustic imaging and synergistic thermoradiotherapy," *ACS Nano*, vol. 11, no. 4, pp. 3990–4001, 2017.

[48] J. D. Obayemi, S. Dozie-Nwachukwu, Y. Danyuo et al., "Biosynthesis and the conjugation of magnetite nanoparticles with luteinizing hormone releasing hormone (LHRH)," *Materials Science and Engineering: C*, vol. 46, pp. 482–496, 2015.

[49] E. Li, X. Cheng, Y. Deng et al., "Fabrication of PEGylated Fe@Bi_2S_3 nanocomposites for dual-mode imaging and synergistic thermoradiotherapy," *Biomaterials Science*, vol. 6, no. 7, pp. 1892–1898, 2018.